ACS APPLIED MATERIALS & INTERFACES

Research Article

www.acsami.org

PPyNT-Im-PtAu Alloy Nanoparticle Hybrids with Tunable Electroactivity and Enhanced Durability for Methanol Electrooxidation and Oxygen Reduction Reaction

Yingjing Peng,[†] Changhai Liu,[‡] Congtao Pan,[†] Lihua Qiu,[†] Suidong Wang,[‡] and Feng Yan*[,†]

[†]Jiangsu Key Laboratory of Advanced Functional Polymer Design and Application, Department of Polymer Science and Engineering, College of Chemistry, Chemical Engineering and Materials Science, and [‡]Jiangsu Key Laboratory of Carbon-Based Functional Materials & Devices, Institute of Functional Nano & Soft Materials (FUNSOM), Soochow University, Suzhou, 215123, China

Supporting Information

ABSTRACT: Polypyrrole nanotubes (PPyNTs)/PtAu alloy nanoparticle (NP) hybrids were synthesized in gram-scale by using covalently attached imidazolium moieties as a linker. The approach involves the surface functionalization of PPyNTs with pendant imidazolium moieties (PPyNT-Im), anion-exchange with Pt and Au precursors, and followed by the reduction of metal ions to produce the PtAu alloy NPs on the surface of PPyNTs. X-ray diffraction (XRD), X-ray photoelectron spectroscopy (XPS), high-angle annular dark-field scanning transmission electron microscopy (HAADF-STEM), and elemental mapping showed that both Pt and Au were atomically distributed in the PtAu alloy NPs without phase segregation. The composition of the PtAu alloy NPs can be simply controlled by adjusting the feed ratio in the metal precursor solution. The electrocatalytic properties of prepared PPyNT-Im-Pt_xAu_y (the suffixes x and y represent the relative molar ratio of Pt and Au in the feed, respectively) NP hybrids were determined by the composition of alloy NPs. The Pt-rich NP hybrids, PPyNT-Im-Pt_8Au_2, showed highly electrocatalytic activity and stability toward the methanol oxidation in both acidic and alkaline solutions, whereas the Au-rich NP hybrids, PPyNT-Im-Pt_2Au_8, showed an enhanced catalytic activity and durability upon oxygen reduction. The present study provided a simple and effective approach for the preparation of PtAu alloy catalysts with controllable composition for high-performance fuel cells and electrochemical sensors.

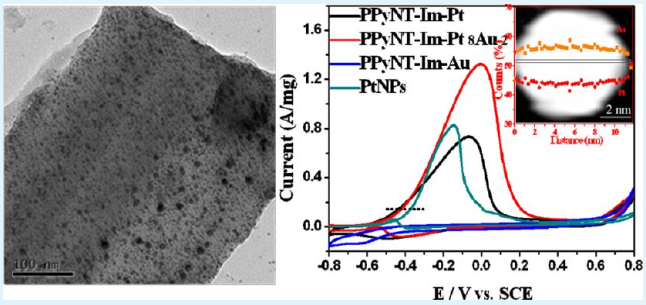

KEYWORDS: *PtAu alloy, polypyrrole nanotubes, electrocatalysts, methanol oxidation, oxygen reduction*

1. INTRODUCTION

The Pt nanoparticles (NPs) with high electrocatalytic activity toward methanol oxidation in direct methanol fuel cells have been extensively investigated in the past years.[1] The overall process involves the adsorption of methanol molecules on the catalyst surface, followed by a complex sequence of reactions leading to the formation of carbon monoxide, which immediately poisoned the electrode under the most of the experimental conditions studied due to the strong bonding of CO on the Pt surface.[2] It has been demonstrated that the composition and morphologies of Pt-based catalysts are important parameters that determine the catalytic activity.[3] To improve the efficiency and the poisoning tolerance ability of the catalysts, reserachers have developed strategies of alloying Pt with other metals or modification of Pt NPs with other species. Pt-based bimetallic alloys, such as PtFe,[4] PtAu,[5] PtNi,[6] PtPd,[7] and PtRu[8] have received a great deal of both academic and industrial attention because of their novel optical, catalytic, electronic, and magnetic properties. Among the Pt-based alloys studied, PtAu bimetallic alloys with various size, composition, and structure have been recently extensively studied because their catalytic properties were different from those of pure Pt and Au, which thus enhancing the catalytic selectivity toward certain products and decreasing the deactivation rate.[9,10]

Recently, many attempts such as the successive reduction (chemical synthesis) or underpotential deposition (electrosynthesis) of Pt and Au precursors have been applied for the preparation of PtAu alloy NPs.[11] For instance, Yamauchi et al. recently reported the electrochemical synthesis of mesoporous PtAu binary alloys using lyotropic liquid crystals (formed from a surfactant solution) containing metal species as the templates.[12] Such an electrochemical template synthesis enabled the preparation of mesoporous PtAu binary alloys without phase segregation, and the composition of PtAu alloy could be controlled by adjusting the compositional ratios of the precursor solution. Although many efforts have been applied for the preparation of bimetallic Pt/Au alloy NPs under various synthetic conditions, most of the reported synthetic processes

Received: February 1, 2013
Accepted: March 7, 2013
Published: March 7, 2013

   dx.doi.org/10.1021/am4004478 | ACS Appl. Mater. Interfaces 2013, 5, 2752−2760

Scheme 1. Reaction Procedure for the Preparation of PPyNT-Im-PtAu NP Hybrids

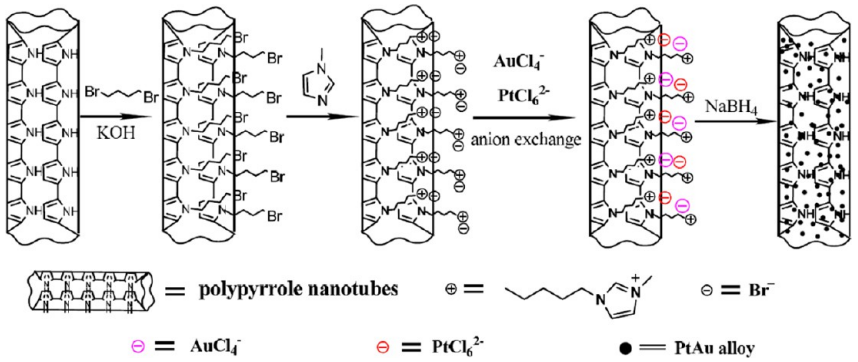

are relatively cost and time-consuming, which limited the large-scale preparation. To date, the synthesis of the binary PtAu alloy is still an open challenge because of the miscibility gap between Pt and Au, according to the binary phase diagram.[13] Therefore, it is still necessary to develop a facile method for the preparation of PtAu alloy nanostructures with desired properties.

Herein, we report a facile and efficient strategy for the dispersion of PtAu alloy NPs on the surface of polypyrrole nanotubes (PPyNTs) with pendant imidazolium moieties as the interlinkers. Compared with carbon nanotubes, PPyNTs can be chemically synthesized in bulk or electrosynthesized in benign media under ambient conditions, especially without the use of high technology and sophisticated instruments. In addition, PPyNTs can be easily modified via the introduction of surface anchoring groups to provide more binding sites.[14,15] The approach reported here mainly involves the surface functionalization of PPyNTs with pendant imidazolium moieties (which introduce a large number of anions to exchange with Pt and Au precursors), and followed by the reduction of the metal ions. The composition of PtAu bimetallic NPs can be simply controlled by the feed ratio of metal precursor and anion-exchange process. X-ray diffraction (XRD), X-ray photoelectron spectroscopy (XPS), high-angle annular dark-field scanning transmission electron microscopy (HAADF-STEM) and elemental mapping clearly showed that both Pt and Au were atomically distributed in the alloy NPs without phase segregation. The resultant PPyNT-Im-Pt_xAu_y (the suffixes x and y represent the relative molar ratio of Pt and Au in the feed, respectively) NP hybrids can be synthesized in gram-scale, and exhibit enhanced electrocatalytic activity toward the methanol oxidation and oxygen reduction. The effect of the element composition and morphology of the synthesized PtAu bimetallic NPs on the electrocatalytic activity was investigated in details.

2. EXPERIMENTAL SECTION

2.1. Materials. Pyrrole, ferric chloride ($FeCl_3$), methyl orange (MO), $HAuCl_4{\cdot}4H_2O$, $H_2PtCl_6{\cdot}6H_2O$, 1-methylimidazole, sodium borohydride ($NaBH_4$), methanol, 1,4-dibromobutane, dimethylformamide (DMF) and polyvinylpyrrolidone (PVP, K-30) were purchased from J&K Scientific Ltd. Pyrrole monomers were distilled under reduced pressure before use. Other chemicals were of analytical grade and used as received without further purification. Deionized water was used for all experiments.

2.2. Characterization. Transmission infrared spectra were recorded on a Nicolet 5200 Fourier transform infrared (FT-IR) in the transmission mode. Energy dispersive X-ray (EDX) spectroscopy was taken on a FEI-quanta 200F scanning electron microscope with acceleration voltage of 20 kV. A TecnaiG 220 transmission electron microscopy (TEM) was used to determine the microstructure of samples. The samples were prepared by placing a drop of diluted latex onto a piece of copper TEM grid and dried at room temperature. The powder X-ray diffraction (XRD) pattern was recorded on a Rigaku D/max 2500 X-ray diffractometer with parallel Cu Kα radiation (λ = 1.54178 Å). XPS spectra were recorded on Kratos Axis Ultra DLD (monochromatic AlKa source of 1486.6 eV in ultrahigh vacuum). High-resolution TEM (HRTEM) was taken on FEI Quanta FRG 200F operating at 200 kV. UV−vis absorption spectra were recorded at room temperature in quartz cells of 1 cm path length using a TU-1800 SPC spectrophotometer. Cyclic voltammetry (CV) experiments were performed on a CHI660C (Chenhua Instrument Company of Shanghai, China) electrochemical workstation with a conventional three-electrode glass cell.

2.3. Synthesis of PPy Nanotubes (PPyNTs). PPyNTs were synthesized using a self-degraded template method as reported in the literature.[16] In a typical procedure, 0.243 g (1.5 mmol) of $FeCl_3$ was dissolved in 30 mL of 5 mM MO solution (0.15 mmol), and a flocculent precipitate appeared immediately. Pyrrole monomer (105 μL, 1.5 mmol) was then added and the mixture was stirred at room temperature for 24 h. The formed PPyNTs were washed with deionized water/ethanol several times until the filtrate was colorless and neutral. The produced PPyNTs were finally dried under vacuum at 60 °C for 24 h.

2.4. Synthesis of PPyNT-Im. A mixture of PPyNTs (0.03 g), KOH powder (0.05 g), and 1,4-dibromobutane (0.14 g) was dispersed in 25 mL DMF and sonicated for 5 min and then held at 60 °C for 24 h under vigorous agitation. The product was filtrated and washed with deionized water and ethanol to thoroughly remove physically absorbed KOH and unreacted 1,4-dibromobutane from the surface of PPyNTs. The product, denoted as PPyNT-$(CH_2)_4$Br, was then dried in a vacuum oven at 60 °C to remove the residual solvent. A mixture containing PPyNT-$(CH_2)_4$Br (0.025 g) and 1-methylimidazole (0.20 g) in 25 mL DMF was sonicated for 5 min and then held at 60 °C for 24 h under vigorous agitation. The product was concentrated and washed with ethanol several times to thoroughly remove the physically absorbed 1-methylimidazole. Then the black precipitate denoted as PPyNT-Im was dried in dynamic vacuum at 60 °C overnight to remove the residual solvent.

2.5. Synthesis of PPyNT-Im-PtAu Hybrids. A mixture containing 1 mg PPyNT-Im and 25 mg PVP was ultrasonicated in 18 mL water until the PPyNT-Im were well-dispersed. The presence of PVP played important roles in determining the size of the alloy NPs.[17] Then the mixed solution containing 0.5 mL of 30 mM H_2PtCl_6 and $HAuCl_4$ solution (0.015 mmol) was then added and the mixture was stirred at room temperature for 3 h. Finally, 2.5 mL of 40 mM $NaBH_4$ (0.1 mmol) solution was added into the reaction mixture and further stirred at room temperature for 3 h until the Pt and Au precursor was reduced completely. The prepared PPyNT-Im-PtAu hybrids were centrifuged, washed thoroughly with deionized water/ethanol, and then dried in dynamic vacuum. PPyNT-Im-Pt and

PPyNT-Im-Au hybrids were synthesized following the procedure of PPyNT-Im-PtAu hybrids.

2.6. Synthesis of Pt NPs. A mixture containing 1.0 mL of 30 mM H_2PtCl_6 (0.03 mmol), 25 mg of PVP, and 18 mL of water was stirred for 5 min at room temperature. Then 4.5 mL of 40 mM $NaBH_4$ (0.18 mmol) was added into the reaction and further stirred at room temperature for 3 h until the Pt precursor was reduced completely. The solution was centrifuged and washed several times with ethanol and deionized water.

2.7. Electrochemical Characterizations. Electrocatalytic characterizations were performed on a CHI660C electrochemical workstation with conventional three-electrode glass cell. A modified glassy carbon (GC) electrode with a diameter of 3 mm and platinum wire were used as working and counter electrode, respectively. A saturated calomel electrode (SCE) was used as the reference electrode. The GC electrode was prepared as follows: prior to the surface coating, the GC electrode was polished carefully with 0.5 μm and then with 0.05 μm alumina powder, and followed by sonicated in 1:1 nitric acid/water (v/v), acetone and in doubly distilled water successively. The surface of GC electrode was allowed to dry under nitrogen atmosphere. The PPyNTs-Im-PtAu was ultrasonically dispersed in the water to form a homogeneous dispersion (1 mg mL^{-1}). The surface of GC electrode was coated with 5 μL of catalyst solution and then dried in air before the electrochemical experiments. All the experiments were carried out at ambient temperature with the potentials respect to SCE.

3. RESULTS AND DISCUSSION

3.1. Synthesis and Characterization of PPyNT-Im-PtAu NP hybrids. Scheme 1 shows the reaction procedure for the preparation of PPyNT-Im-PtAu NP hybrids. PPyNTs were synthesized follow a self-degraded template method as reported in the literature.[16] The synthesized PPyNTs were then surface functionalized with imidazolium moieties as shown in Scheme 1. The resultant imidazolium-functionalized PPyNTs were characterized by Fourier transform infrared spectroscopy (see the Supporting Information, Figure S1). As it can be seen that the characteristic absorption bands at 2850, 2920, and 2955 cm^{-1} arise from the $-(CH_2)_4-$ moieties. An absorption peak at 1634 cm^{-1} assigned to the vibrational mode of 1-methyl imidazolium cations were observed, which indicates that imidazolium cations have been grafted onto the surface of pristine PPyNTs.[18] The Br^- anions of the pendant imidazolium moieties were then exchanged with $PtCl_6^{2-}$ and $AuCl_4^-$, and followed by the reduction with $NaBH_4$ to produce the PPyNT-Im-Pt_xAu_y NP hybrids in gram scale.

The morphology and microstructure of PPyNT-Im-PtAu hybrids were examined with the transmission electron microscopy (TEM). Figure 1 shows the typical TEM images of the synthesized PPyNT-Im-Pt_xAu_y NP hybrids at low and high magnifications, respectively. It can be clearly seen that high-density and well-dispersed metal NPs have been deposited on the PPyNT-Im surface. It is supposed that imidazolium moieties played a key role in dispersing alloy NPs on PPyNTs. For comparasion, NPs gregated to lager size in the surface of unmodified PPyNTs (see the Supporting Information, Figure S2). The Pt NPs with a mean diameter of about 4.1 nm were deposited on the surface of PPyNTs (Figure 1A, 1A′). It should be noted that the size of PtAu NPs increase with the increasing Au ratio (see Figure 1B–D). The pure Au NPs with a mean diameter of ~13.2 nm were synthesized (shown in Figure 1E, E′).

The critical element composition of the PtAu alloy NPs deposited on the PPyNT surface was investigated by energy-dispersive X-ray (EDX) spectroscopy (see the Supporting Information, Figure S3), and the results are summarized in

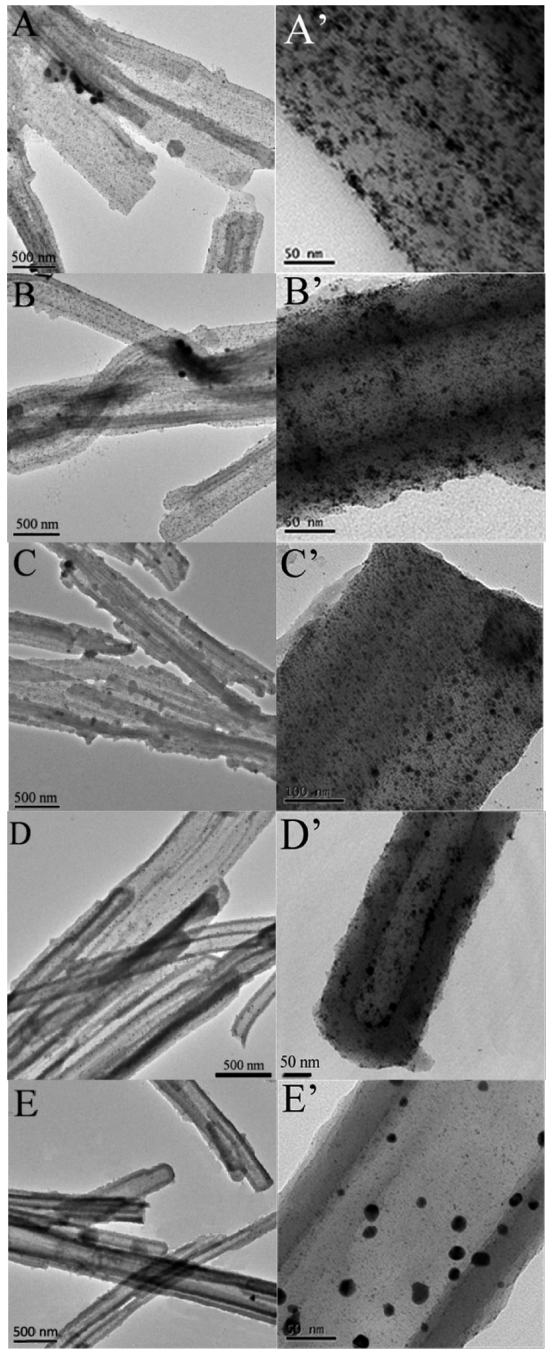

Figure 1. TEM images of (A, A′) PPyNT-Im-Pt, (B, B′) PPyNT-Im-Pt_8Au_2, (C, C′) PPyNT-Im-Pt_5Au_5, (D, D′) PPyNT-Im-Pt_2Au_8, and (E, E′) PPyNT-Im-Au hybrids at different magnifications.

Table 1. It can be seen that all the PPyNT-Im-PtAu NP hybrids are composed of desired metals. The determined molar ratio of Pt/Au of each sample closely matched the feed ratio, indicating that the loading of PtAu NPs on the PPyNT surface could be easily controlled by adjusting the molar ratio of $PtCl_6^{2-}$ and $AuCl_4^-$ anions during the anion-exchange reaction. It is supposed that the formation of small and well-dispersed PtAu alloy NPs on the PPyNT-Im surface is due to the surface functionized imidazolium moieties which play an important role in the coupling of the counteranions ($PtCl_6^{2-}$ and $AuCl_4^-$) through electrostatic interaction and coordination. The low interfacial tension of the imidazolium cations on the surface of

Table 1. Metal Composition of the PPyNT-Im-Pt_xAu_y NP Hybrids

sample	Pt/Au ratio	
	theoretical	experimental (EDX detection)
PPyNT-Im-Pt	1:0	1:0
PPyNT-Im-Pt_8Au_2	8:2	7.65:2.35
PPyNT-Im-Pt_5Au_5	5:5	4.52:5:48
PPyNT-Im-Pt_2Au_8	2:8	1.46:8:54
PPyNT-Im-Au	0:1	0:1

PPyNTs promoted the nucleation rate of PtAu alloy NPs, and allowing the formation of small NPs because of the low rates of Ostwald ripening.[19] The loading mass of produced Pt_xAu_y NPs on the PPyNT surface was determined by thermogravimetric analyzer (TGA) in the air atmosphere (see the Supporting Information, Figure S4). The results of TGA show that 28.9, 36.4, 37.9, 40.1, and 40.7 (wt %) of Pt NPs, Pt_8Au_2, Pt_5Au_5, Pt_2Au_8 alloy NPs, and Au NPs were deposited on the PPyNTs surface, respectively.

The presence of PtAu alloy NPs with the different Pt/Au nominal atomic ratios ranged from 1:0 to 0:1 deposited on the PPyNTs surface was further confirmed by powder X-ray diffraction (XRD) as shown in Figure 2A. All the samples show a broad peak at 2θ = 23.6° may be ascribed to the doped PPy main chains of the PPyNTs (not shown in Figure 2A).[20] Figure 2A(a) show the XRD patterns of Pt NPs deposited on PPyNTs. The face-centered cubic (fcc) structure of Pt was confirmed by the presence of diffraction peaks at 39.61, 46.31, 67.41, and 81.31°, which are assigned to Pt(111), Pt(200), Pt(220), and Pt(311), respectively, suggesting that the face-centered cubic platinum NPs were synthesized and deposited on the PPyNTs surface. Similar results were observed for the face-centered cubic Au NPs deposited on the PPyNTs surface either (Figure 2A(e)). In addition, four diffraction peaks corresponding to the PtAu(111), (200), (220) and (311) planes indicate that PtAu NP alloys with a face-centered cubic structure have been synthesized (Figure 2A(b–d)).[21] With the increase of Au ratio, the peak positions of 2θ (111), (200), (220), (311) slightly shift to lower degree. For example, the 2θ (111) peaks for PPyNT-Im-Pt, PPyNT-Im-Pt_8Au_2, PPyNT-Im-Pt_5Au_5, PPyNT-Im-Pt_2Au_8 and PPyNT-Im-Au are 39.930, 38.354, 38.236, 38.212, and 37.930° (see the Supporting Information, Table S1), respectively. These results reveal the possible interaction between Pt and Au alloys, indicating that the PtAu NP alloys, not just a mixture of Pt and Au NPs, have been synthesized in this work. The average size of the metal NPs was calculated based on the half-peak width of 2θ (111), using Scherrer's equation: $d = 0.9\,\lambda/\beta\,\cos\theta_{max}$ (see Table S1 in the Supporting Information). Where d is the average size of the NPs, λ is the X-ray wavelength (Cu Kα λ = 1.54178 Å), θ_{max} is the diffraction angle at the peak position, and β is the full width at half-maximum in radians. It can be seen from Table S1 in the Supporting Information that the sizes of PtAu NPs alloy (9.2–13.3 nm) are smaller than that of pure Au NPs (14.1 nm), and larger than pure Pt NPs (4.4 nm). The results of XRD further confirm the synthesis of PtAu NPs alloy.

X-ray photoelectron spectroscopy (XPS) spectra have been widely used to identify the surface elemental compositions and the chemical state of materials. Figure 2B shows the full XPS spectra of PPyNT-Im-Au, PPyNT-Im-Pt, and PPyNT-Im-Pt_8Au_2. Distinct to PPyNT-Im-Au and PPyNT-Im-Pt, both Pt and Au elements were detected on the surface of PPyNT-Im-Pt_8Au_2. The Pt state of the PPyNT-Im-Pt_8Au_2 was further studied by Pt 4f XPS (Figure 2C). It can be seen that the peak shape of Pt 4f is different from that of metallic Pt (Pt^0), indicating that Pt exists in multiple chemical states in the PPyNT-Im-Pt_8Au_2 alloy NPs. The most intense component of Pt 4f signal occurs at 70.8 and 74.1 eV is corresponding to Pt^0. The higher energy signal, which is located at 71.9 and 75.2 eV, can be attributed to Pt^{2+} species (e.g., PtO and $Pt(OH)_2$), whereas the highest energy signal peaks at 73.6 and 76.6 eV are attributed to Pt^{4+} species. The signals of Pt oxide species are observed possibly because of the interaction between Pt and O and imidazolium moieties.[11,22]

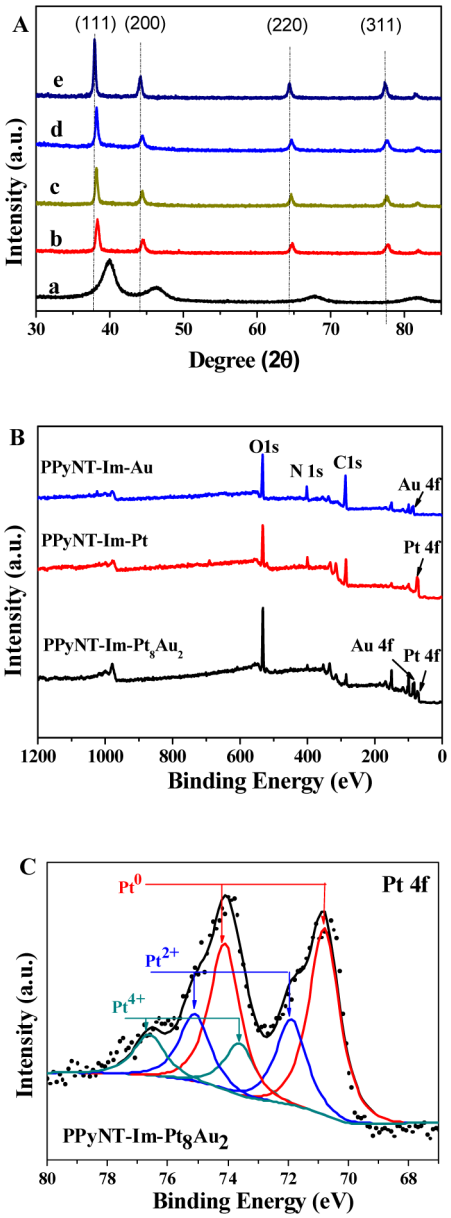

Figure 2. (A) XRD patterns for (A-a) PPyNT-Im-Pt, (A-b) PPyNT-Im-Pt_8Au_2, (A-c) PPyNT-Im-Pt_5Au_5, (A-d) PPyNT-Im-Pt_2Au_8, and (A-e) PPyNT-Im-Au; and (B) XPS spectra for PPyNT-Im-Au, PPyNT-Im-Pt, PPyNT-Im-Pt_8Au_2, and (C) Pt 4f XPS spectru of PPyNT-Im-Pt_8Au_2 fitted by three pairs of curves.

Images A and B in Figure 3 show the HRTEM and high-angle annular dark-field scanning TEM (HAADF-STEM) of a single PtAu NP, respectively. Upon the basis of HRTEM shown

dx.doi.org/10.1021/am4004478 | ACS Appl. Mater. Interfaces 2013, 5, 2752–2760

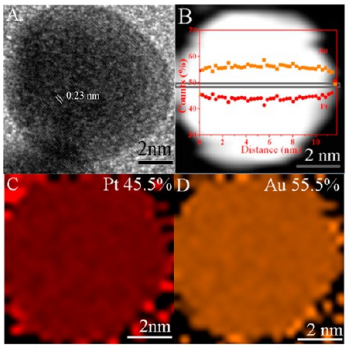

Figure 3. (A) HRTEM images, (B) HAADF-STEM (inset shows the cross-sectional compositional line profiles of the square areas), and (C, D) elemental mappings for alloy NPs deposited on PPyNT-Im-Pt_5Au_5.

in Figure 3A, it can be seen that the high crystalline particles with apparently well-defined lattice fringes were presented, which agrees quite well with the results of XRD analysis. Moreover, the lattice fringes for the NP is measured to be 0.23 nm, corresponding to the (111) planes of face-centered cubic Pt and Au, indicating that (111) plane is the mainly exposed face and the PtAu NPs have been initially identified as a metal alloy of Pt and Au atoms.[9a,23] From the line-scanning profile across the particle, it can be more clearly visualized that the Pt and Au were well-dispersed without any phase separations on the nanometer scale (inset of Figure3B). These results further demonstrate the successful formation of PtAu alloy NPs, and the Pt/Au ratio was in good agreement with that obtained from the EDX analysis (see Figure S3 in the Supporting Information).

Figure 4A shows the UV−vis absorption spectra of PPyNT-Im-Pt_xAu_y NP hybrids dispersed in water. The peak at around 280 nm was contributed to the absorption of PPyNT-Im. In the case of PPyNT-Im-Au, an absorption peak at 560 nm contributed by the absorption of Au NPs was observed.[24] Since Pt NPs do not show any absorption in the UV−vis spectra,[25] blue-shift and weakened absorption peaks of PPyNT-Im-PtAu alloy NP hybrids were observed with the increasing Pt ratio. The observed spectral changes could be directly observed in the color changes of the aqueous solution. Figure 4B shows the photograph of aqueous dispersions containing 0.1 mM PPyNT-Im-Au, PPyNT-Im-Pt_xAu_y, and PPyNT-Im-Pt. It was found that the synthesized PPyNT-Im-PtAu hybrids can be well dispersed in water and exhibit the expected various color due to the mutual interface effect between Au and Pt.[26]

3.2. Methanol Electrooxidation on PPyNT-Im-PtAu NP Hybrids. Pt and Pt-based catalysts have been applied as the electrocatalysts for methanol electrooxidation.[27,28] However, the poor tolerance of carbon monoxide limited application of Pt catalysts to the development of direct methanol fuel cells (DMFCs). Here, the electrocatalytic properties of the PPyNT-Im-Pt_xAu_y NP hybrids as potential electrocatalysts for methanol electrooxidation were examined.

Figure 5A shows the cyclic voltammograms (CVs) of PPyNT-Im-Pt_xAu_y NP hybrids. The electrochemical surface area (ECSA) of all the catalysts was measured by using hydrogen adsorption−desorption peak area and calculated by integrating the charge passing the electrode during the hydrogen adsorption/desorption process after the correction for the double-layer formation, according to the following equation:

$$\mathrm{ECSA} = \frac{Q_H}{0.21 \times L_{Pt}}$$

Where Q_H (mC cm^{-2}) represents the mean value between the amounts of charge exchanged during the electro-adsorption and desorption of H_2 on Pt sites, L_{Pt} is the Pt loading (mg cm^{-2}) on the GC electrode and 0.21 (mC cm^{-2}) represents the charge required to oxidize a monolayer of H_2 on Pt. The calculated ECSA values of all the catalysts are listed in Figuer 5B. It has been demonstrated that the ECSA value of the catalyst is related to electrocatalytic activity toward methanol oxidation.[29] Here, the ECSA value of the PPyNT-Im-Pt_xAu_y hybrids increases with increasing Pt ratio of the alloy NPs. For example, the ECSA of PPyNT-Im-Pt_5Au_5, PPyNT-Im-Pt_8Au_2 and PPyNT-Im-Pt are 66.4, 74.3, and 72.0 $m^2\ g^{-1}$ of Pt, respectively. However, it should be noted that the ECSA value of PPyNT-Im-Pt_8Au_2 (74.3 m^2g^{-1} of Pt) is even higher than that of PPyNT-Im-Pt (72.0 $m^2\ g^{-1}$ of Pt), indicating a higher electrocatalytic activity of PPyNT-Im-Pt_8Au_2 hybrids.

Figures 5C,D show the CV curves of the PPyNT-Im-Pt and PPyNT-Im-Pt_8Au_2 modified GC electrodes after 500 and 1000 CV cycles. It can be seen that the current densities of the peaks in the hydrogen adsorption/desorption potential regions (−0.2−0.0 V) for the PPyNT-Im-Pt decreased dramatically with increase of CV cycles. On the contrary, PPyNT-Im-Pt_8Au_2 showed a high electrocatalytic stability under the same experimental conditions, and retained most of the initial electrocatalytic activity even after 1000 CV cycles. A current peak at about 0.2 V may associate to the reduction of Au-CO generated during the methanol oxidation and another current peak at 0.5 V corresponded to the reduction of Pt oxide species

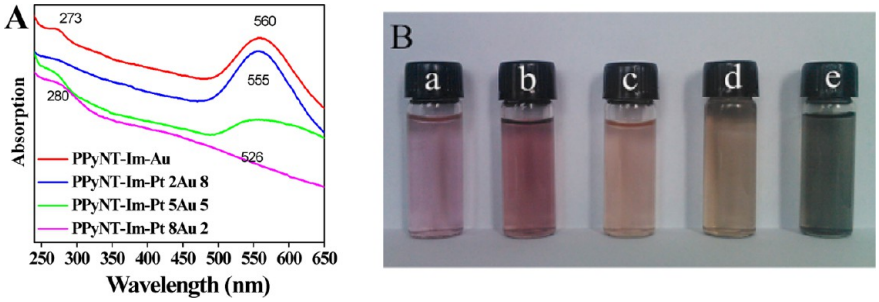

Figure 4. (A) UV−vis absorption spectra of PPyNT-Im-Pt_8Au_2, PPyNT-Im-Pt_5Au_5, PPyNT-Im-Pt_2Au_8, and PPyNT-Im-Au hybrids dispersed in water. (B) Photograph of colloidal aqueous solution containing 0.1 mM (a) PPyNT-Im-Au, (b) PPyNT-Im-Pt_2Au_8, (c) PPyNT-Im-Pt_5Au_5, (d) PPyNT-Im-Pt_8Au_2, and (e) PPyNT-Im-Pt hybrids.

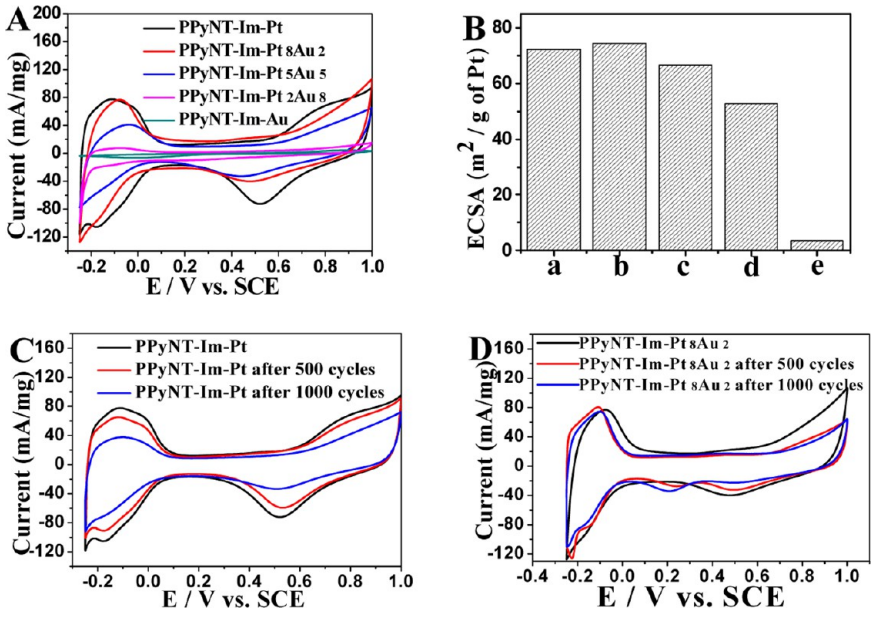

Figure 5. (A) CV curves and (B) the calculated ECSA values for (a) PPyNT-Im-Pt, (b) PPyNT-Im-Pt_8Au_2, (c) PPyNT-Im-Pt_5Au_5, (d) PPyNT-Im-Pt_2Au_8, and (e) PPyNT-Im-Au; and CV curves for (C) PPyNT-Im-Pt, (D) PPyNT-Im-Pt_8Au_2 before and after different cycles of CV test. The CV tests were carried out at 50 mV s^{-1} at room temperature.

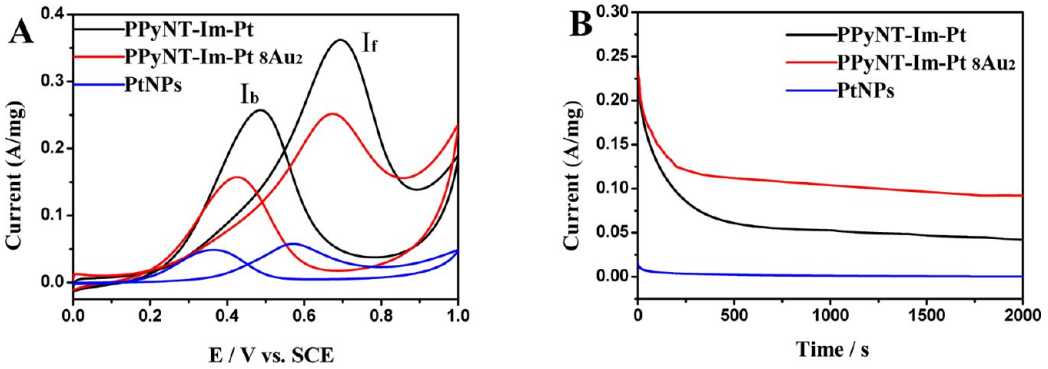

Figure 6. (A) CVs (Scan rate: 50 mV s^{-1}), and (B) potential-dependent steady-state current of PPyNT-Im-Pt, PPyNT-Im-Pt_8Au_2 and Pt NPs hybrids for methanol oxidation at 0.6 V (vs SCE). All the measurements were conducted in N_2-saturated 0.5 M H_2SO_4 + 0.5 M CH_3OH solution.

are observed (Figure 5D).[30] With the increase in CV cycles, the peak current of Pt oxide species decreased while the peak of Au oxide species increased (Figure 5D). The results indicate that during the CV cycles, the generated CO adsorpted on Au instead of Pt in the alloy NPs, which therefore resisted the poisoning of Pt and retained the electroactivity of the PtAu alloy NPs. The results discussed above demonstrated an enhanced catalytic durability of PPyNT-Im-Pt_8Au_2 probably due to the possible synergetic effect of Pt and Au metallic components.

Figure 6 shows the CVs of PPyNT-Im-Pt and PPyNT-Im-Pt_8Au_2 NP hybrids in a N_2-saturated 0.5 M H_2SO_4 solution containing 0.5 M methanol. For comparison, pure Pt NPs (~4 nm) was also characterized under the same experimental conditions. The electrooxidation of methanol of PPyNT-Im-Pt, PPyNT-Im-Pt_8Au_2, and Pt NPs in acid is characterized by two well-defined current peaks on the forward and reserve scans. As can be seen from Figure 6A that the peak current of PPyNT-Im-Pt (0.36 A mg^{-1}) and PPyNT-Im-Pt_8Au_2 (0.25 A mg^{-1}) is 6.0 and 4.2 times higher than that of pure Pt NPs (0.06 A mg^{-1}). The ratio of the forward oxidation current peak (I_f) to the reverse current peak (I_b), I_f/I_b, is an important index of the catalyst tolerance to the carbonaceous species accumulation, Pt═C═O.[31] Here the I_f/I_b value is calculated to be 1.82 for PPyNT-Im-Pt, 2.22 for PPyNT-Im-Pt_8Au_2 and 1.17 for Pt NPs, respectively. The highest I_f/I_b value of PPyNT-Im-Pt_8Au_2 indicated that more effective oxidation of methanol occurs and most of intermediate carbonaceous species have been oxidized to CO_2 during the forward potential scan when the Au was added into the alloy catalysts.[9b,18,32]

Figure 6B shows the chronoamperometric profiles of PPyNT-Im-Pt, PPyNT-Im-Pt_8Au_2 and Pt NPs. It can be clearly seen that the current density for PPyNT-Im-Pt reached a steady value after about 300 s, however, kept decreasing even after 1000 s. The decay of current density for methanol oxidation of PPyNT-Im-Pt_8Au_2 is significantly slower than that of PPyNT-Im-Pt, indicating a higher tolerance to the carbonaceous species generated during methanol oxidation. In addition, the steady-state current density for PPyNT-Im-Pt_8Au_2 is about 2.0 times higher than that for PPyNT-Im-Pt, indicating that PPyNT-Im-Pt_8Au_2 has a higher electroactivity for methanol oxidation.[33]

Therefore, the catalytic activity of PPyNT-Im-Pt_8Au_2 toward the methanol oxidation in alkaline solution was also investigated in this work.[34] Figure 7A shows the CV curves

dx.doi.org/10.1021/am4004478 | ACS Appl. Mater. Interfaces 2013, 5, 2752−2760

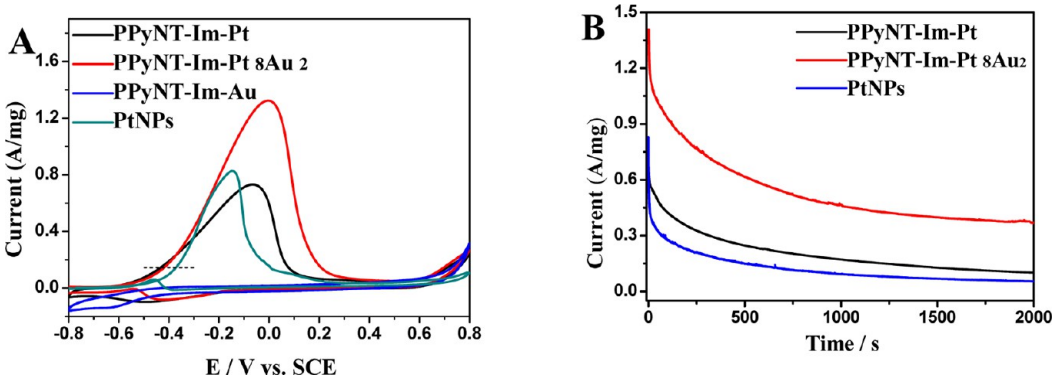

Figure 7. (A) CVs of PPyNT-Im-Pt, PPyNT-Im-Pt_8Au_2, PPyNT-Im-Au hybrids and Pt NPs (Scan rate: 50 mV s^{-1}); (B) Potential-dependent steady-state current of PPyNT-Im-Pt, PPyNT-Im-Pt_8Au_2 and Pt NPs hybrids for methanol oxidation at −0.2 V (vs SCE). All the measurements were conducted in N_2-saturated 0.5 M NaOH + 0.5 M CH_3OH solution at room temperature.

of PPyNT-Im-Pt, PPyNT-Im-Pt_8Au_2, PPyNT-Im-Au, and Pt NPs (~4 nm) in N_2-saturated 0.5 M NaOH + 0.5 M CH_3OH solution. It can be seen that the PPyNT-Im-Au hybrids shows a poor electrocatalytic activity toward methanol oxidation. Compared with PPyNT-Im-Pt and Pt NPs catalysts; however, a dramatic enhancement of the peak current can be observed on PPyNT-Im-Pt_8Au_2 hybrid catalysts. Furthermore, as indicated by dotted lines shown in Figure 7A that the corresponding onset potential of PPyNT-Im-Pt_8Au_2 for methanol oxidation in alkaline environment is much lower than that of Pt NPs, indicating an excellent electrocatalytic activity of the PPyNT-Im-Pt_8Au_2 hybrids toward the oxidation of methanol in alkaline condition which may due to the electrocatalytic ability promoted by Au in base electrolyte toward methanol oxidation.[35] However, the catalyst PPyNT-Im-Pt_5Au_5 and PPyNT-Im-Pt_2Au_8 show no electrocatalytic activity toward methanol oxidation. These results are consistent with those of ECSA values shown in Figure 5. Such an excellent electrocatalytic property enable PPyNT-Im-Pt_8Au_2 NP hybrids to be an effective and cheap cathodic electrocatalyst for alkaline DMFCs.

The chronoamperometric profiles of PPyNT-Im-Pt, PPyNT-Im-Pt_8Au_2 and Pt NPs are presented in Figure 7B. Under a giving potential of −0.2 V, PPyNT-Im-Pt_8Au_2 shows a higher initial current and a slower decay of the current with the time increasing suggesting a highly catalytic activity and poisoning-tolerance ability. The steady-state polarization curve for PPyNT-Im-Pt_8Au_2 is about 3.4 and 6.3 times higher as that for PPyNT-Im-Pt hybrids and pure Pt NPs at 2000 s, respectively, indicating that the PPyNT-Im-Pt_8Au_2 hybrids have an excellent electrocatalytic activity toward the electro-oxidation of methanol in alkaline condition.

3.3. Electroreduction of Oxygen on PPyNT-Im-PtAu NP Hybrids. The catalyst oxygen reduction reaction (ORR) is an important reaction in life processes and in energy converting systems (such as fuel cells).[20,36] Here, the electrochemical properties of the as-prepared catalyst are also investigated by catalyzing the oxygen reduction in alkaline media.

Figure 8 exhibits the typical linear sweep voltammetry and potential-dependent steady-state current of PPyNT-Im-Au, PPyNT-Im-Pt_5Au_5, PPyNT-Im-Pt_2Au_8, and PPyNT-Im-Pt hybrids in O_2-saturated 0.5 M NaOH aqueous solution. As indicated by dotted lines shown in Figure 8A, the corresponding potential of PPyNT-Im-Pt_2Au_8 is lower than those of the PPyNT-Im-Pt, PPyNT-Im-Pt_5Au_5 and PPyNT-Im-Au at a given oxidation current density. The chronoampero-

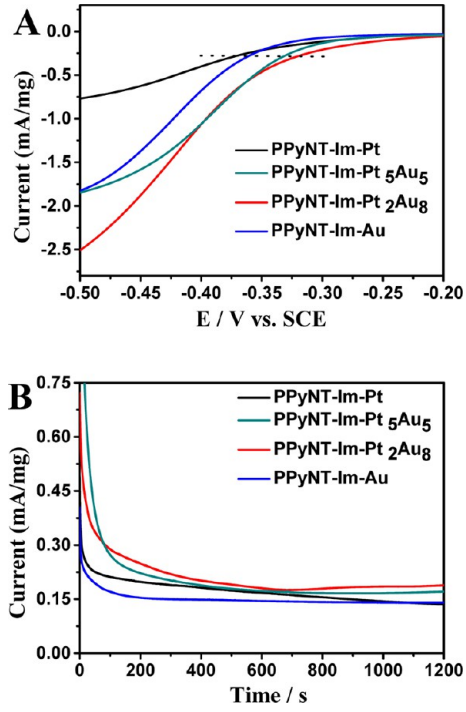

Figure 8. (A) Linear sweep voltammetry and (B) potential-dependent steady-state current of PPyNT-Im-Pt, PPyNT-Im-Pt_5Au_5, PPyNT-Im-Pt_2Au_8, and PPyNT-Im-Au hybrids in O_2-saturated 0.5 M NaOH aqueous solution at room temperature. Scan rate: 20 mV s^{-1}.

metric profiles of PPyNT-Im-Pt, PPyNT-Im-Pt_5Au_5, PPyNT-Im-Pt_2Au_8 and PPyNT-Im-Au, are presented in Figure 8B. Under a giving potential of −0.5 V, PPyNT-Im-Pt_2Au_8 shows a higher initial current and a slower decay of the current with the time increasing. These results confirm that PPyNT-Im-Pt_2Au_8 hybrids exhibit much enhanced catalytic activity toward oxygen reduction in alkaline solution. PPyNT-Im-Pt_2Au_8 shows the highest catalytic activity and poisoning-tolerance ability toward oxygen reduction due to the presence of Au thus provides highly efficient utilization of Pt. The catalytic properties of Pt-containing nanostructures are strongly dependent on the particle shape that could be only obtained with complicated methods.[37] The majority of Pt atoms remain unexposed and unavailable for catalysis. Therefore, the PPyNT-Im-Pt catalyst keeps low activity toward the ORR. Moreover, the weak chemisorption properties of Au NPs due to the filled d-band

dx.doi.org/10.1021/am4004478 | ACS Appl. Mater. Interfaces 2013, 5, 2752−2760

lead to the low catalytic activity of PPyNT-Im-Au hybrids. Meanwhile, the alloy nanostructures may change the density of states of d-band of pure Au NPs so that PPyNT-Im-Pt_2Au_8 hybrids is more beneficial to combine with O_2 molecular and having highest catalytic performance.[38]

4. CONCLUSIONS

In summary, a facile strategy for synthesis of PtAu alloys with different ratios deposited on PPyNTs surface using imidazolium moieties as the surface linkers was investigated in this work. The covalently attached imidazolium moieties play an important role in coupling of the metal anions through electrostatic interaction and coordination. The composition of the PtAu alloy NPs can be simply controlled by adjusting the feed ratio in the metal precursor solution. The resultant PPyNT-Im-Pt_xAu_y NPs show selective electrocatalytic activity toward the methanol oxidation (Pt-rich alloy NPs) and oxygen reduction reaction (Au-rich alloy NPs), depending on the alloy components. The present study provided a simple and effective approach for the development of high-performance PtAu alloy catalysts for fuel cells or electrochemical sensors.

■ ASSOCIATED CONTENT

Supporting Information

FTIR spectra, TGA, and EDX characterization of synthesized hybrids. This material is available free of charge via the Internet at http://pubs.acs.org/.

■ AUTHOR INFORMATION

Corresponding Author

*E-mail: fyan@suda.edu.cn.

Notes

The authors declare no competing financial interest.

■ ACKNOWLEDGMENTS

This work was supported by Natural Science Foundation of China (No. 21274101), National Basic Research Program of China (973 Program) (2012CB825800), The Natural Science Foundation of Jiangsu Province (BK2011274), Research Fund for the Doctoral Program of Higher Education (20103201110003), and the Project Funded by the Priority Academic Program Development of Jiangsu Higher Education Institutions.

■ REFERENCES

(1) Meng, H.; Xie, F.; Chen, J.; Sun, S.; Shen, P. K. *Nanoscale* **2011**, *3*, 5041−5048.
(2) Kuai, L.; Wang, S.; Geng, B. *Chem. Commun.* **2011**, *47*, 6093−6095.
(3) Si, F.; Ma, L.; Liu, C.; Zhang, X.; Xing, W. *RSC Adv.* **2012**, *2*, 401−403.
(4) (a) Nakaya, M.; Kanehara, M.; Yamauchi, M.; Kitagawa, H.; Teranishi, T. *J. Phys. Chem. C* **2007**, *111*, 7231−7234. (b) Poh, C. K.; Tian, Z. Q.; Gao, J. J.; Liu, Z. L.; Lin, J. Y.; Feng, Y. P.; Su, F. B. *J. Mater. Chem.* **2012**, *22*, 13643−13652.
(5) (a) Hernández-Fernández, P.; Rojas, S.; Ocón, P.; Gómez de la Fuente, J. L.; San Fabián, J.; Sanza, J.; Peña, M. A.; García-García, F. J.; Terreros, P.; Fierro, J. L. G. *J. Phys. Chem. C* **2007**, *111*, 2913−2923. (b) Wang, L.; Yamauchi, Y. *Chem. Mater.* **2011**, *23*, 2457−2465. (c) Huang, J.; Hou, H.; You, T. *Electrochem. Commun.* **2009**, *11*, 1281−1284.
(6) Qiu, H.; Li, L.; Lang, Q.; Zou, F.; Huang, X. *RSC Adv.* **2012**, *2*, 3548−3554.
(7) (a) Kobayashi, H.; Yamauchi, M.; Kitagawa, H.; Kubota, Y.; Kato, K.; Takata, M. *J. Am. Chem. Soc.* **2008**, *130*, 1818−1819. (b) Li, Y.; Wang, Z. W.; Chiu, C.-Y.; Ruan, L.; Yang, W.; Yang, Y.; Palmer, R. E.; Huang, Y. *Nanoscale* **2012**, *4*, 845−851.
(8) Ye, F.; Yang, J.; Hu, W.; Liu, H.; Liao, S.; Zeng, J.; Yang, J. *RSC Adv.* **2012**, *2*, 7479−7486.
(9) (a) Zhu, C.; Guo, S.; Dong, S. *Adv. Mater.* **2012**, *24*, 2326−2331. (b) Guo, S.; Dong, S.; Wang, E. *ACS Nano* **2009**, *4*, 547−555. (c) Liu, B.; Ren, W.; Li, S.; Liu, C.; Cheng, H.-M. *Chem. Commun.* **2012**, *48*, 2409−2411. (d) Kusada, K.; Yamauchi, M.; Kobayashi, H.; Kitagawa, H.; Kubota, Y. *J. Am. Chem. Soc.* **2010**, *132*, 15896−15898.
(10) (a) Wang, J.; Thomas, D. F.; Chen, A. *Chem. Commun.* **2008**, 5010−5012. (b) Xu, J.; Zhao, T.; Liang, Z.; Zhu, L. *Chem. Mater.* **2008**, *20*, 1688−1690.
(11) Zhang, J.; Oko, D. N.; Garbarino, S.; Imbeault, R.; Chaker, M.; Tavares, A. C.; Guay, D.; Ma, D. *J. Phys. Chem. C* **2012**, *116*, 13413−13420.
(12) Yamauchi, Y.; Tonegawa, A.; Komatsu, M.; Wang, H.; Wang, L.; Nemoto, Y.; Suzuki, N.; Kuroda, K. *J. Am. Chem. Soc.* **2012**, *134*, 5100−5109.
(13) Nakamura, T.; Herbani, Y.; Sato, S. *J. Nanopart. Res.* **2012**, *14*, 1−9.
(14) (a) Yang, X.; Li, L.; Shang, S.; Pan, G.; Yu, X.; Yan, G. *Mater. Lett.* **2010**, *64*, 1918−1920. (b) Yang, X.; Li, L.; Yan, F. *Sens. Actuators, B* **2010**, *145*, 495−500.
(15) (a) Xiao, W.; Sun, Z.; Chen, S.; Zhang, H.; Zhao, Y.; Huang, C.; Liu, Z. *RSC Adv.* **2012**, *2*, 8189−8193. (b) Guo, S.; Dong, S.; Wang, E. *Adv. Mater.* **2010**, *22*, 1269−1272. (c) Wu, B.; Hu, D.; Kuang, Y.; Liu, B.; Zhang, X.; Chen, J. *Angew. Chem., Int. Ed.* **2009**, *48*, 4751−4754.
(16) Yang, X. M.; Zhu, Z. X.; Dai, T. Y.; Lu, Y. *Macromol. Rapid Commun.* **2005**, *26*, 1736−1740.
(17) Sun, Y.; Xia, Y. *Science* **2002**, *298*, 2176−2179.
(18) Qiu, L.; Liu, B.; Peng, Y.; Yan, F. *Chem. Commun.* **2011**, *47*, 2934−2936.
(19) (a) Mu, X.-d.; Meng, J.-q.; Li, Z.-C.; Kou, Y. *J. Am. Chem. Soc.* **2005**, *127*, 9694−9695. (b) Clement, N. D.; Cavell, K. J.; Jones, C.; Elsevier, C. J. *Angew. Chem., Int. Ed.* **2004**, *43*, 1277−1279. (c) Dupont, J.; Spencer, J. *Angew. Chem., Int. Ed.* **2004**, *43*, 5296−5297.
(20) Qiu, L.; Peng, Y.; Liu, B.; Lin, B.; Peng, Y.; Malik, M. J.; Yan, F. *Appl. Catal., A* **2012**, *413*−*414*, 230−237.
(21) Wang, D.; Xin, H. L.; Wang, H.; Yu, Y.; Rus, E.; Muller, D. A.; DiSalvo, F. J.; Abruña, H. D. *Chem. Mater.* **2012**, *24*, 2274−2281.
(22) (a) Sen, S.; Sen, F.; Gokagac, G. *Phys. Chem. Chem. Phys.* **2011**, *13*, 6784−6792. (b) Zhang, X.; Chan, K.-Y. *Chem. Mater.* **2002**, *15*, 451−459.
(23) Chai, J.; Li, F.; Hu, Y.; Zhang, Q.; Han, D.; Niu, L. *J. Mater. Chem.* **2011**, *21*, 17922−17929.
(24) He, J.; Zhang, P.; Gong, J.; Nie, Z. *Chem. Commun.* **2012**, *48*, 7344−7346.
(25) Xu, Y.; Dong, Y.; Shi, J.; Xu, M.; Zhang, Z.; Yang, X. *Catal. Commun.* **2011**, *13*, 54−58.
(26) Guo, S.; Li, J.; Dong, S.; Wang, E. *J. Phys. Chem. C* **2010**, *114*, 15337−15342.
(27) (a) Liu, H.; Song, C.; Zhang, L.; Zhang, J.; Wang, H.; Wilkinson, D. P. *J. Power Sources* **2006**, *155*, 95−110. (b) Murray, E. P.; Tsai, T.; Barnett, S. A. *Nature* **1999**, *400*, 649−651.
(28) (a) Liang, H.-P.; Zhang, H.-M.; Hu, J.-S.; Guo, Y.-G.; Wan, L.-J.; Bai, C.-L. *Angew. Chem., Int. Ed.* **2004**, *43*, 1540−1543. (b) Yu, X.; Kuai, L.; Geng, B. *Nanoscale* **2012**, *4*, 5738−5743.
(29) Luo, Z.; Yuwen, L.; Bao, B.; Tian, J.; Zhu, X.; Weng, L.; Wang, L. *J. Mater. Chem.* **2012**, *22*, 7791−7796.
(30) (a) Xia, B. Y.; Wu, H. B.; Wang, X.; Lou, X. W. *J. Am. Chem. Soc.* **2012**, *134*, 13934−13937. (b) Zhang, L.; Li, N.; Gao, F.; Hou, L.; Xu, Z. *J. Am. Chem. Soc.* **2012**, *134*, 11326−11329.
(31) (a) Shan, C.; Tang, H.; Wong, T.; He, L.; Lee, S.-T. *Adv. Mater.* **2012**, *24*, 2491−2495. (b) Ding, L.-X.; Wang, A.-L.; Li, G.-R.; Liu, Z.-Q.; Zhao, W.-X.; Su, C.-Y.; Tong, Y.-X. *J. Am. Chem. Soc.* **2012**, *134*, 5730−5733.

(32) Yang, X.; Yang, Q.; Xu, J.; Lee, C.-S. *J. Mater. Chem.* **2012**, *22*, 8057−8062.
(33) Pan, C.; Qiu, L.; Peng, Y.; Yan, F. *J. Mater. Chem.* **2012**, *22*, 13578−13584.
(34) (a) Singh, B.; Murad, L.; Laffir, F.; Dickinson, C.; Dempsey, E. *Nanoscale* **2011**, *3*, 3334−3349. (b) Lin, B.; Qiu, L.; Lu, J.; Yan, F. *Chem. Mater.* **2010**, *22*, 6718−6725.
(35) Zhang, J.; Sasaki, K.; Sutter, E.; Adzic, R. R. *Science* **2007**, *315*, 220−222.
(36) (a) Gao, M.-R.; Gao, Q.; Jiang, J.; Cui, C.-H.; Yao, W.-T.; Yu, S.-H. *Angew. Chem., Int. Ed.* **2011**, *50*, 4905−4908. (b) Shim, J. H.; Kim, J.; Lee, C.; Lee, Y. *Chem. Mater.* **2011**, *23*, 4694−4700. (c) Stephens, I. E. L.; Bondarenko, A. S.; Gronbjerg, U.; Rossmeisl, J.; Chorkendorff, I. *Energy Environ. Sci.* **2012**, *5*, 6744−6762. (d) Wang, C.; Chi, M.; Wang, G.; van der Vliet, D.; Li, D.; More, K.; Wang, H.-H.; Schlueter, J. A.; Markovic, N. M.; Stamenkovic, V. R. *Adv. Funct. Mater.* **2011**, *21*, 147−152. (e) Dong, S.; Chen, X.; Wang, S.; Gu, L.; Zhang, L.; Wang, X.; Zhou, X.; Liu, Z.; Han, P.; Duan, Y.; Xu, H.; Yao, J.; Zhang, C.; Zhang, K.; Cui, G.; Chen, L. *ChemSusChem* **2012**, *5*, 1712−1715. (f) Oh, J. G.; Oh, H. S.; Lee, W. H.; Kim, H. *J. Mater. Chem.* **2012**, *22*, 15215−15220.
(37) Zhang, G.-R.; Zhao, D.; Feng, Y.-Y.; Zhang, B.; Su, D. S.; Liu, G.; Xu, B.-Q. *ACS Nano* **2012**, *6*, 2226−2236.
(38) Kuai, L.; Yu, X.; Wang, S.; Sang, Y.; Geng, B. *Langmuir* **2012**, *28*, 7168−7173.